Simplified Speed Control of Permanent Magnet Synchronous Motors Using Genetic Algorithms

Hicham Chaoui, *Senior Member, IEEE*, Mehdy Khayamy, Okezie Okoye, and Hamid Gualous, *Member, IEEE*

***Abstract*—In this paper, a simplified control scheme is introduced for permanent magnet synchronous motors (PMSMs). The control strategy consists of a direct voltage controller that capitalizes on the motor's model to achieve accurate speed tracking. As such, no explicit currents loop regulation is needed which simplifies the control structure and unlike other control strategies, no motor's parameter knowledge, voltage or current transducer is required. But, the absence of current regulation loops yields higher energy consumption, which limits the motor's range of operation. Therefore, a genetic algorithm is presented to determine control gains with optimal current consumption ensuring operation at the full range of the machine. Simulation and experimental results for different situations highlight the performance of the proposed controller in transient, steady-state, and standstill conditions. Furthermore, the simplicity of the control scheme makes it a good candidate for a low-cost implementation of real-time PMSM drives.**

***Index Terms*—Direct voltage control, genetic algorithm (GA), permanent magnet synchronous motors (PMSMs).**

I. Introduction

THE HIGH efficiency and torque–inertia ratio of the variable speed permanent magnet synchronous motor (PMSM), coupled with its high power density and low rotor losses, has contributed in making it a preferred solution in industrial applications [1]–[3]. In spite of its numerous high-performance applications, its control is challenging and has been a focus of continuing research in the academia. It is desired to be able to achieve precise and robust control of the motor in the face of varying operating conditions, model parameter variations, friction nonlinearities, unmodeled uncertainties, and external disturbances.

Due to the nonlinearities associated with its multivariable nature, the control scheme of the PMSM should be such that its

Manuscript received December 30, 2017; revised February 26, 2018 and April 26, 2018; accepted June 18, 2018. Date of publication June 28, 2018; date of current version February 20, 2019. Recommended for publication by Associate Editor A. K. Gupta. *(Corresponding author: Hicham Chaoui.)*

H. Chaoui is with the Intelligent Robotic and Energy Systems Research Group, Department of Electronics, Carleton University, Ottawa, ON K1S 5B6, Canada (e-mail:

of this approach, however, is that its robustness is dependent upon selection of large control gains, while large gains, in turn, cause the chattering phenomenon [22]. To cope with nonlinear factors and parameter variations in PMSM drives, adaptive speed control schemes have been presented in [23]–[26]. However, in most of these techniques, the authors only consider load torques and structured parameter variations without reckoning with the system's unmodeled dynamics. Also, in real world applications, it may be burdensome to formulate mathematical models for the complex industrial processes in which these PMSM drives are employed. Certain factors like temperature, and noise are inherently unpredictable but may yet interfere with the control process.

Another interesting class of control methodology that is fast gaining grounds is soft-computing control, which uses tools such as artificial neural networks and fuzzy logic systems. Artificial neural networks have been favored due to their ability to accurately approximate complex relationships between a set of inputs and outputs; a relationship that may be highly nonlinear, unpredictable, and subject to uncertainties [27]. Hence, they have been used in applications where a robust control scheme model is required, but they are difficult to derive analytically [28]–[32]. These soft-computing controllers, however, exhibit excellent performance at the cost of being computationally expensive [33]. This complicates the control algorithm and makes their practical implementation not trivial.

The contribution of this paper is a simplified direct voltage control strategy for PMSM speed tracking. Direct voltage control yields significant complexity reduction with respect to classical cascaded-based control structures that use current regulating loops. Currents transformation from the natural reference frame to the synchronously rotating reference frame entails carrying out Clarke and Park transform with sine and cosine operations, which increase the computation burden on the processor. Besides simplicity, the measurement of the noisy motor's voltages and currents is not required as in most of the PMSM-based controllers, which favors better convergence and tracking and reduces the number of sensors with respect to other methods. Making the control highly dependent on various sensors increases potential failure points, which reduces the system's reliability. Thus far, very few attempts of direct voltage control have been proposed for PMSMs [34]–[40]. But, they either require dc-link current sensing, inner stabilizing loop, or an advanced fuzzy logic controller. Studies have shown that the absence of current sensing and control limits the motor's range of operation since it results in a higher energy consumption, which raises the urgency of finding optimum operation points with minimum current [37], [38]. Unlike in surface mount PMSMs, finding such optimum operation points for interior PMSMs (IPMSMs) is much more challenging and only an approximation can be found [39], [40]. Moreover, tuning a direct voltage controller in such as a way to obtain optimal operation in the presence of various uncertainties is not an easy task to undertake [40]. Henceforth, a simplified direct voltage control strategy is proposed. To pinpoint its optimal control gains that yield a minimal current consumption, a genetic algorithm (GA) based optimization technique is also proposed. The derivation of the control strategy is presented for both surface mount and IPMSMs. The rest of the paper is organized as follows. Section II outlines the PMSM model and details the proposed control scheme. To properly evaluate the effectiveness of any new speed control algorithm for PMSMs, it is appropriate to compare its performance to the well-established FOC as commonly done in [41]–[45]. To this end, in Section III, simulation and experimental results are reported and discussed, and comparison with the standard FOC is carried out. Finally, the paper is concluded with some remarks.

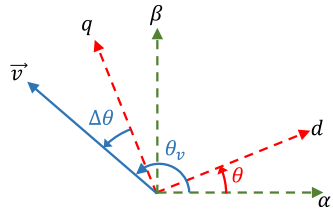

Fig. 1. Spatial representation of the applied voltage vector in reference frames.

II. PMSM Dynamics and Control Strategy

The mathematical model of a PMSM defined in the synchronously rotating reference frame d–q can be expressed by [38]

$$v_d = Ri_d + L_d\frac{d}{dt}i_d - L_q p\omega i_q \tag{1a}$$

$$v_q = Ri_q + L_q\frac{d}{dt}i_q + L_d p\omega i_d + p\lambda\omega \tag{1b}$$

$$\tau = \frac{3}{2}p[(L_d - L_q)i_d i_q + \lambda i_q]. \tag{1c}$$

The mechanical equations of motion can be described by

$$\frac{d}{dt}\omega = \frac{1}{J}(\tau - \tau_F - \tau_L) \tag{2a}$$

$$\frac{d}{dt}\theta = p\omega \tag{2b}$$

where v_d, v_q, and i_d, i_q are the stator voltage and current in d–q coordinates, L_d, L_q is the inductance in d–q coordinates, R is the armature winding resistance, λ is the flux linkage, p is the number of pole pairs, J is the rotor and load inertia, ω is the rotor mechanical speed, θ is the rotor electrical angle, τ, τ_F, and τ_L are motor, friction, and load torques, respectively.

The spatial relationship between the α–β stationary frame, the synchronously rotating d–q frame, and the applied voltage vector is shown in Fig. 1.

Under the assumption of unknown nonlinear system's dynamics and with only θ and ω as system's measurable states, the objective is to design a control law v and $\Delta\theta$ to force the motor's speed ω to track its predefined time-dependent desired values ω^*. The motor's parameters, R, L_d, L_q, p, λ, J, F_v, τ_F, and τ_L are also assumed to be *a priori* unknown. Let $e_\omega = \omega - \omega^*$ denotes the motor speed error, with ω^* being the desired time-dependent speed signal. The control strategy uses the voltages v_α and v_β that are fed to a space vector pulsewidth modulation (SVPWM) algorithm to produce the proper duty cycles for the inverter (see Fig. 2). The motor's voltage drop due to the

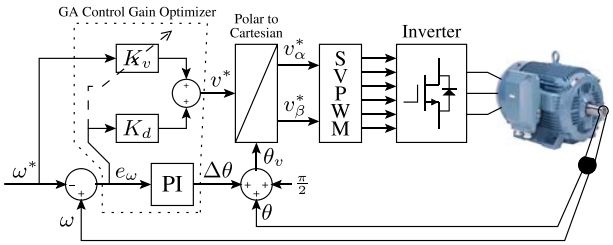

Fig. 2. Block diagram of the proposed control scheme.

armature winding resistance is negligible so that the motor's voltage amplitude and angle at steady state can be written as

$$\begin{aligned} v &= \sqrt{v_d^2 + v_q^2} \\ &= \sqrt{(L_q p\omega i_q)^2 + \left((L_d i_d + \lambda)p\omega\right)^2} \end{aligned} \tag{3}$$

$$\begin{aligned} \Delta\theta &= -\tan^{-1}\left(\frac{v_d}{v_q}\right) \\ &= \tan^{-1}\left(\frac{L_q p\omega i_q}{L_d p\omega i_d + \lambda p\omega}\right). \end{aligned} \tag{4}$$

Conventional controllers achieve speed tracking by regulating d–q currents to generate the needed d–q voltages. In the absence of current control, the introduction of a load torque causes excessive current consumption due to the lack of current angle control. Setting $i_d = 0$ leads to a maximum torque–current ratio, also called maximum torque per ampere (MTPA), for surface-mount PMSMs and simplifies the control for IPMSMs. Therefore

$$v = \omega\sqrt{(pL_q)^2 i_q^2 + (p\lambda)^2} \tag{5}$$

$$\Delta\theta = \tan^{-1}\left(\frac{L_q}{\lambda} i_q\right). \tag{6}$$

Substituting $i_d = 0$ in (1c) makes the generated torque linearly proportional to the q-axis current expressed as

$$i_q = \frac{2}{3p\lambda}\tau. \tag{7}$$

Substituting i_q in (5) and (6) leads to

$$v = \omega\sqrt{\left(\frac{2L_q}{3\lambda}\right)^2 \tau^2 + (p\lambda)^2} \tag{8}$$

$$\Delta\theta = \tan^{-1}\left(\frac{2L_q}{3p\lambda^2}\tau\right). \tag{9}$$

Equation (8) reveals a linear relationship between the applied voltage amplitude and the motor's speed at no load, i.e., $\tau \to 0$. In this case, $v = K\omega$ and $\Delta\theta = 0$ with $K = p\lambda$. As torque increases, the slope of the linear relationship, i.e., K, raises from a gentle gradient to much steeper inclination. It is also noteworthy from (9) the nonlinear relationship between the applied voltage angle and the motor's torque. It can also be concluded that $\Delta\theta$ should vary from 0 to $\frac{\pi}{2}$.

For the IPMSM, rotor saliency makes MTPA achievable by a certain combination of the d–q axes currents. Due to the embedded permanent magnets, the rotor becomes a salient pole

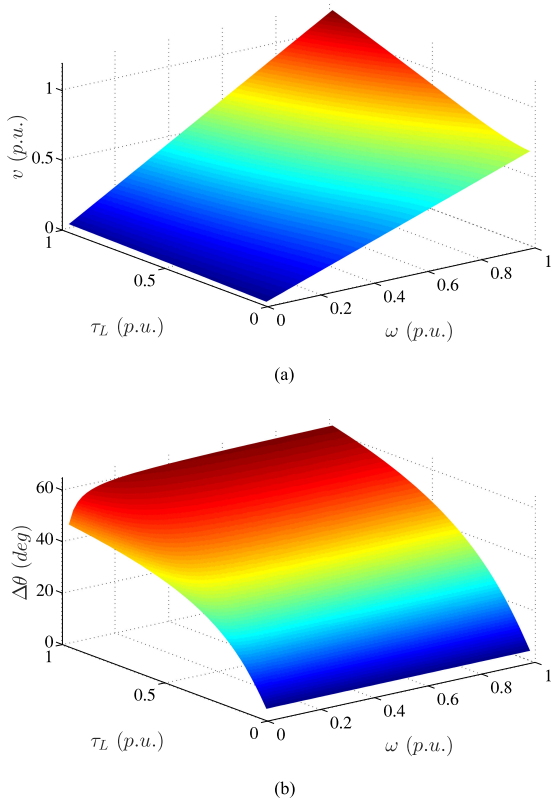

Fig. 3. IPMSM MTPA voltage amplitude/angle versus speed and torque load. (a) Amplitude. (b) Angle.

making use of both magnetic and reluctance torques. To minimize the stator current amplitude, the derivative of the torque is taken with respect to the current angle, which leads to a much complicated dynamics [46]. In this case, the relationship between the motor's voltage amplitude and angle with respect to its speed and torque can be solved numerically as it is illustrated in Fig. 3. The relationship between the amplitude of the applied voltage and the speed of the motor is depicted in Fig. 3(a). At no load, the amplitude of the applied voltage varies linearly with the speed of the IPMSM. The slope of this variation is magnified as torque increases toward its rated value, which is consistent with the resultant voltage amplitude dynamics (8). On the other hand, Fig. 3(b) reveals that the voltage angle of the IPMSM varies as inverse tangent function of the electromagnetic torque. This behavior is also described in the motor's voltage angle dynamics (9). It is important to note that due to the nature of the inverse tangent function, any small uncertainty on the motor's parameters would lead to a significant angle deviation. Hence, an exact mathematical representation that relies on the motor's parameters cannot be efficiently applied in this case. Additionally, the torque is not directly measurable. Therefore, this nonlinear relationship is approximated using a simple PI controller. At this stage, the control law can be defined as

$$v^* = \hat{K}_v\, \omega^* + K_d\, e_\omega \tag{10}$$

$$\Delta\theta = K_p\, e_\omega + K_i \int e_\omega \tag{11}$$

Algorithm 1: Genetic Algorithm.

begin
- Generate randomly a population of n solutions.

repeat
- Calculate fitness function for each solution.

repeat
- Select best pair of parent solutions.
- Form two offsprings with a crossover probability.
- Mutate two offsprings at each locus with a mutation probability.
- If n is odd, one new population member can be discarded at random.

until *n offsprings have been created*;

until *satisfactory fitness level is reached*;

Algorithm 2: Proposed Control Algorithm.

begin
- **Step 1:** Find control gains via GA optimization.

repeat
- **Step 2:** Measure rotor feedback position using resolver, and calculate speed.
- **Step 3:** Calculate the speed error e_ω.
- **Step 4:** Use Equation (12) to calculate $\hat{K}_v$.
- **Step 5:** Calculate v^* from Equation (10).
- **Step 6:** Get $\Delta\theta$ from Equation (11).
- **Step 7:** Get θ_v by adding $\Delta\theta$ to rotor angle measured in Step 2.
- **Step 8:** Convert voltage amplitude and angle from polar to Cartesian.
- **Step 8:** Generate modulation indexes using SVPWM.

until *stop request is received*;

where $\hat{K}_v$ is an adaptive gain since the slope between the applied voltage and the speed is not constant (see Fig. 3(a)), K_d is a constant gain that adds robustness to the adaptation loop, and K_p, K_i are the proportional and integral control gains, respectively. The adaptive gain $\hat{K}_v$ is updated using the following adaptation law

$$\dot{\hat{K}}_v = -\eta\, \omega^*\, e_\omega \tag{12}$$

where η is a positive constant adaptation gain that defines the convergence speed. It is important to note that (12) is inspired from adaptive control theory, which adjusts *a priori* unknown coefficient using a gradient descent technique. Henceforth, the applied voltage can be written as

$$v^*_{\alpha\beta} = v^* \angle \theta_v \tag{13}$$

where v^* is the amplitude of the voltage applied to the motor and $\theta_v = \theta + \frac{\pi}{2} + \Delta\theta$ is its total angle to go from the α-axis to the applied voltage (Fig. 1). In the absence of current sensing, low power factor operation is reported in [47], which yields higher motor's energy consumption (i.e., reactive power). According to the IPMSM MTPA operation characteristics (see Fig. 3), there exists a set of voltage amplitude and angle that yields minimal current consumption. The proposed adaptive control scheme needs a careful selection of its control gains K_p, K_i, K_d, and η to provide the right balance between voltage amplitude and angle, which is not trivial considering the number of possible combinations.

As a powerful tool capable of providing robust approximation for systems that may be subjected to uncertainties, GA is ideal for the task thanks to its search and adaptation capabilities. This heuristic search technique is inspired by evolutionary biology with nature selection phenomenon as an adaptation mechanism [48]. This mechanism consists of the use of candidate solutions, called elements of population, represented in a binary form, called chromosomes. The adaptation is done with moving from one population of chromosomes to a new population by using natural selection genetic inspired operators of crossover, mutation, and inversion. In each generation, the fitness of every individual in the population is evaluated and the selection operator chooses the chromosomes in the population (based on their fitness) that are allowed to reproduce evolving toward better solutions. The new population is then used in the next generation, and the process usually terminates when a satisfactory fitness level has been reached for the population.

In this paper, the GA involves three types of operators: selection, crossover (single point), and mutation. The selection operator selects chromosomes with the best fitness level in the population for reproduction. Crossover mimics a biological recombination between two single chromosome organisms. The subsequences of two chromosomes exchange before and after a randomly chosen locus to form two offsprings. For example, the crossover after the third locus of chromosomes 01000101 and 11111111 produce the two offspring 01011111 and 11100101. On the other hand, mutation randomly toggles a chromosome bit. Since the control algorithm does not employ any current regulation loop, the right pair of voltage amplitude–angle pair is needed to ensure optimal consumption. These gains are carefully chosen using GA described in Algorithm 1, since an arbitrary set of gains would result in bad consumption. The cost function is chosen based on the motor variable one seeks to minimize. Since minimal current consumption is desired, while achieving accurate tracking is desired in this case, the cost function has been defined as a weighted sum of the integral of the speed error and the integral of the current consumption. More specifically, it is given by $f(x) = \rho \int e_\omega + (1-\rho) \int i$, where ρ defines a compromise between tracking and current consumption and i is the current amplitude. The optimal gains for the controller can be arrived at by starting with a large initial population, and running the optimization for a sufficiently high number of iterations. However, this optimization procedure is conducted offline and is not part of the control cycle. Also, this strategy eliminates the heavy computational burden that is usually associated to computational intelligence-based controllers in general. Chromosomes are coded into 16 bits, which offers a good tradeoff between computation and precision. On the other hand, the number of populations is set to 15 chromosomes for fast convergence to the optimal solution.

TABLE I
MOTOR'S PARAMETERS

Parameter	Value
Nominal power (HP)	$P_n = 10$
Nominal speed (RPM)	$w_n = 1800$
Nominal torque (N·m)	$\tau_n = 39.5$
Inductance in d-axis (H)	$L_d = 22.1 \cdot 10^{-3}$
Inductance in q-axis (H)	$L_q = 91.1 \cdot 10^{-3}$
Armature winding resistance (Ω)	$R = 6.51 \cdot 10^{-1}$
Flux linkage (Wb)	$\lambda = 67.09 \cdot 10^{-2}$
Rotor and load inertia (kg·m^2)	$J = 1 \cdot 10^{-1}$
Number of pole pairs	$p = 2$

III. SIMULATION AND EXPERIMENTAL RESULTS

A. Setup

To validate the effectiveness of the proposed control strategy, different simulations and experiments are carried out on a 10 HP, 1800 r/min IPMSM (Table I). The simulation is carried out in Matlab/Simulink environment. A dc power supply generates a regulated 750 V dc-link voltage as a supply to a 10 kW IGBT-based inverter (Fig. 4). Switching and sampling frequencies are set to 1 kHz and 20 kHz, respectively. A 10 HP induction motor is used in torque control mode as a mechanical load. The speed measurement is obtained by a resolver (800123-5-A) with 10 Vrms 4.5 kHz voltage as the input excitation of the primary winding and 5 V_{rms} on the output sine and cosine windings. Opal-RT software, running on OP4500 real-time processor with 16 bit A/D, is used to synthesize the angle and speed from feedback signals of the resolver. The reference speed signal is taken as a ramp, which is commonly used as step signals to study the convergence properties of a variety of control systems. The performance of the proposed controller is studied considering the motor's speed and reference signals, three-phase currents, currents on d–q axes, electromagnetic torque, and the control signal, i.e., applied voltage $v^*_{\alpha\beta}$. The gains of the controller are set to $K_p = 6.5 \times 10^{-3}$, $K_i = 1.1$; $\eta = 4 \times 10^{-13}$, and $K_d = 2.3 \times 10^{-3}$.

B. Results

The proposed control strategy is compared in both simulation and experimentally against the well-known MTPA FOC technique used as a benchmark for a maximum torque–current ratio. Results are presented in Figs. 5 and 6. In both cases, the speed of the IPMSM is first ramped to the rated value of 1800 r/min. At steady state, a load torque of 22 N·m is applied to the motor. The proposed control strategy is able to restore the speed of the motor to its rated value with a current consumption of less than 10 A as seen in both simulation and experimental results (see Figs. 5(d) and 6(d)). Worthy of note is the fact that this current consumption is almost identical to that of MTPA FOC as observed in Figs. 5(c) and 6(c). While comparison shows similar performance at steady state, a slight current overshoot is observed during acceleration. This is mainly due to the use of a linear PI controller to compensate for the PMSM's nonlinear dynamics. This rational choice was made for simplicity and performance under these conditions can be improved with the use of a nonlinear controller. Fig. 6(c) and (d) shows unbalanced currents for both control methods, which is due to current sensors' imprecision.

TABLE II
EXPERIMENTAL PERFORMANCE METRICS

	MTPA FOC	Proposed method
IAE	0.68	0.52
ITAE	4.83	3.37
EFF	100%	98%

Upon introduction of the torque load, a momentary speed deviation is observed. Although good tracking performance is achieved by vector control (see Fig. 6(a)), some electromagnetic torque oscillations are observed in Fig. 6(e). The proposed method is able to cope with the unexpected load while providing smoother control effort as it is illustrated in Fig. 6(h), which yields higher quality currents and electromagnetic torque (see Fig. 6(d) and (f)). The high efficiency potential of the proposed strategy is clearly demonstrated in this experiment. It is noteworthy that this performance is achieved with the use of current sensing or regulation. Furthermore, the simplicity of the proposed methodology is astonishing as opposed to cascaded-based controllers available in the literature. Hence, the real-time computation burden of the proposed method is lower due to elimination of current regulators, decoupling elements, and dq transformation of the currents.

To better assess the performance of the proposed control scheme, two quantitative tracking performance metrics are introduced, i.e., the integral of absolute error (IAE) and the integral of time absolute error (ITAE), and one more quantitative performance metric is introduced as the integral of the three-phase current. These metrics are measured as follows:

$$\text{IAE} = \int_{t_0}^{t_f} |e| dt \tag{14a}$$

$$\text{ITAE} = \int_{t_0}^{t_f} t|e| dt \tag{14b}$$

$$\text{EFF} = \int_{t_0}^{t_f} I_{abc} dt \tag{14c}$$

where t_0 and t_f are initial and final time instants, respectively. The obtained numeric values for these performance metrics are displayed in Table II. Comparison is carried-out with respect to the MTPA FOC, which is considered as a benchmark. As such, the proposed control method yields 98% efficiency without the use of current sensing or control. It is worthwhile noting that further improvement is possible by replacing the PI controller

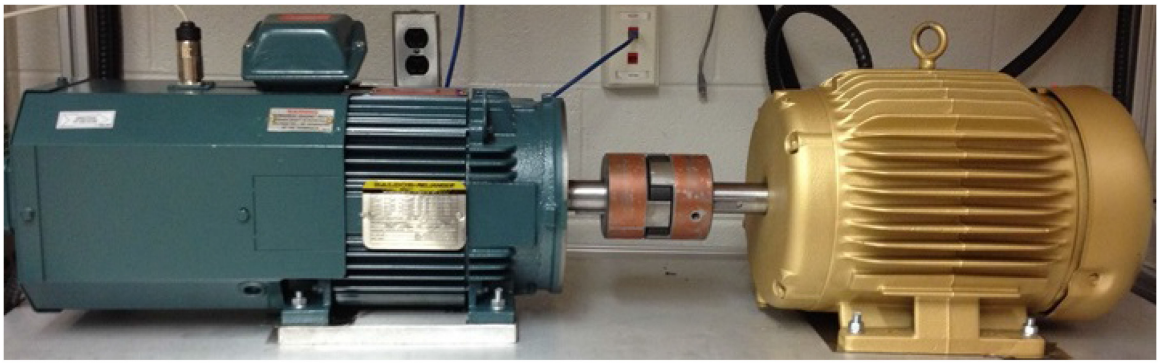

(a)

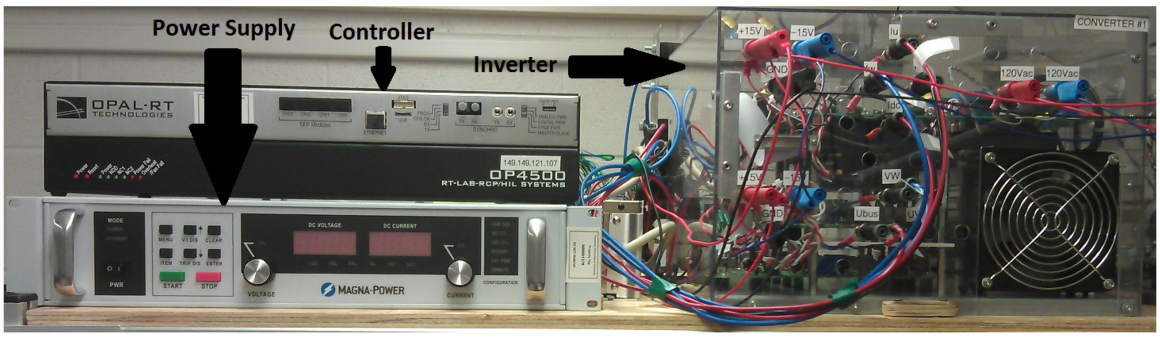

(b)

Fig. 4. Experimental setup. (a) AC motors. (b) Opal-RT real-time control platform, dc power supply, and inverter.

with an advanced control technique at the expense of added design complexity and computation. On the other hand, the proposed controller's simplicity leads to a higher tracking accuracy shown by both tracking performance metrics, i.e., IAE and ITAE.

To better show the effectiveness of the proposed control approach, another experimental comparison is performed against the MTPA FOC at a lower load torque. Using the same speed reference trajectory, the proposed method and the MTPA FOC are subjected to a 13 N·m load torque and results are displayed in Fig. 7. As it can be observed, the MTPA FOC shows good tracking performance (see Fig. 7(a)) and few oscillations (see Fig. 7(e)). On the other hand, smoother signals are reported with the proposed method (see Fig. 7(f)). Most importantly, both methods yield similar current consumption (see Fig. 7(c) versus Fig. 7(d)). Then, the ability of the proposed approach to cope with another operating condition while maintaining good performance and low current usage is evaluated.

The torque ripple is evaluated for both control methods under different load torque conditions and switching frequencies. Under 13 N·m load torque, results reveal 7.69% and 5.38% torque ripple, respectively, with switching frequencies of 5 kHz and 8 kHz. The same frequencies yield 6.81% and 4.36% respectively for 22 N·m load torque. As it can be noticed, torque ripple decreases as the load and the switching frequency increase.

To further demonstrate the effectiveness of the proposed control method at different operating conditions, various loads are applied at different speeds. For that, the speed reference is set to 500 r/min and load torques of 5 N·m and 15 N·m are applied at 5 s interval. Then, the speed is ramped up to 1000 r/min, and the same load profile is applied again. For comparison, the same speed/load profile is also used for the MTPA vector control. Results for both methods are depicted in Fig. 8. As it is revealed, the controller shows good speed tracking performance with a similar current consumption as MTPA FOC.

Remark 1: To extend the controller's operation to field weakening region, the machine's voltage should be limited to its rated value. To do that, a saturation is required on the adaptive k_v, which is simple compared to cascaded control techniques. Since GA selects control gains with the best fitness function, any control gain combination that would result in instability is naturally eliminated. After optimization, selected gains can be used to analyze the gain and phase margins of the overall control system. On another aspect, the proposed control strategy has several advantages, but also has limitations. For instance, the limited ability of the PI controller in handling nonlinearities is observed by current transient spikes that can be decreased with the use of an advanced control technique at the expense of added design complexity and computation. Designing a direct voltage controller that provides the right balance between voltage amplitude and angle is challenging. To extend this work, future plans may envision evaluating field weakening operation along with thorough comparison against other control techniques such as, DTC and MPC.

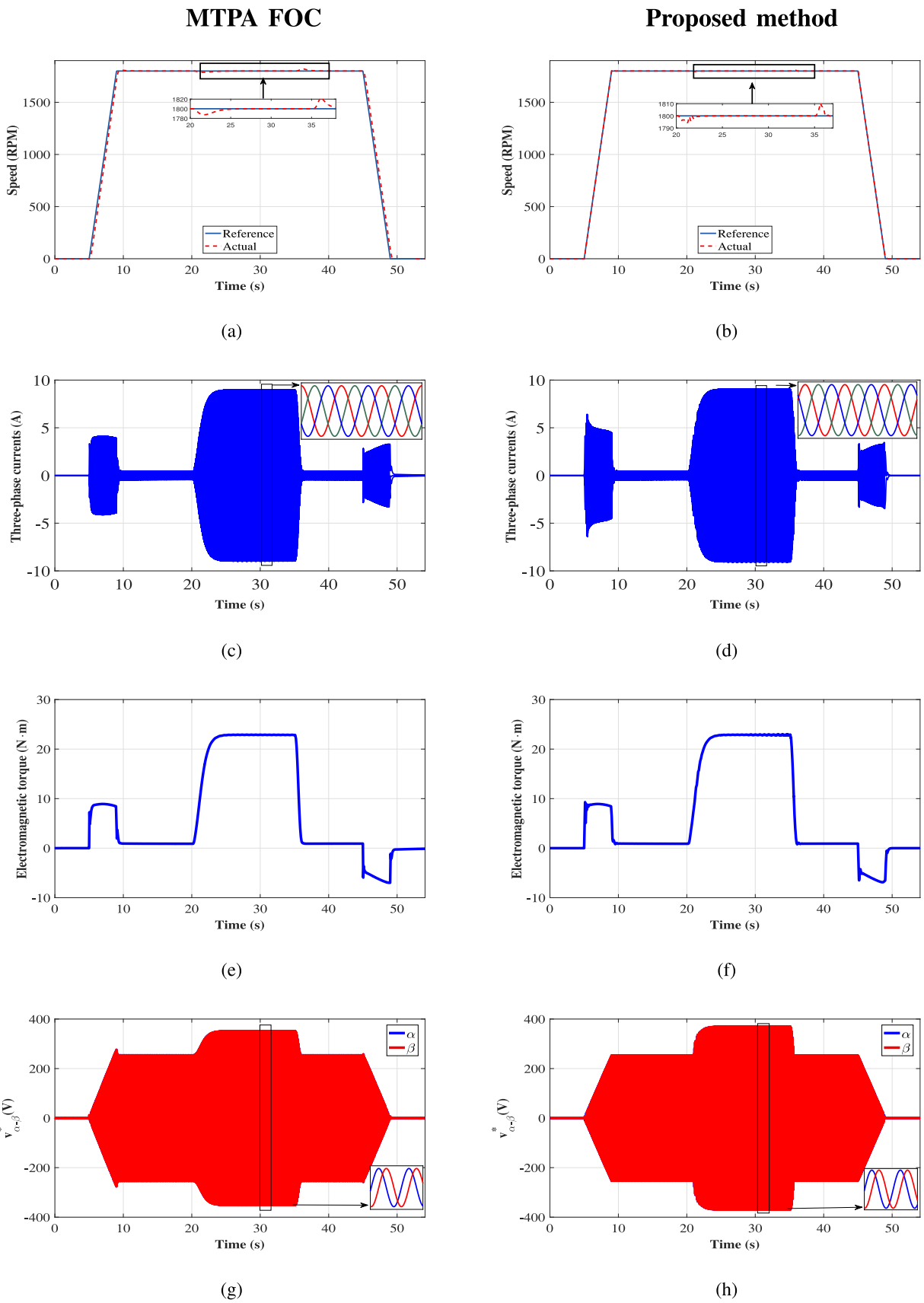

Fig. 5. Simulation results under 22 N·m at 1800 r/min. (a), (b) Reference and actual speed signals. (c), (d) Three-phase currents. (e), (f) Torque. (g), (h) Control voltages in the α–β reference frame.

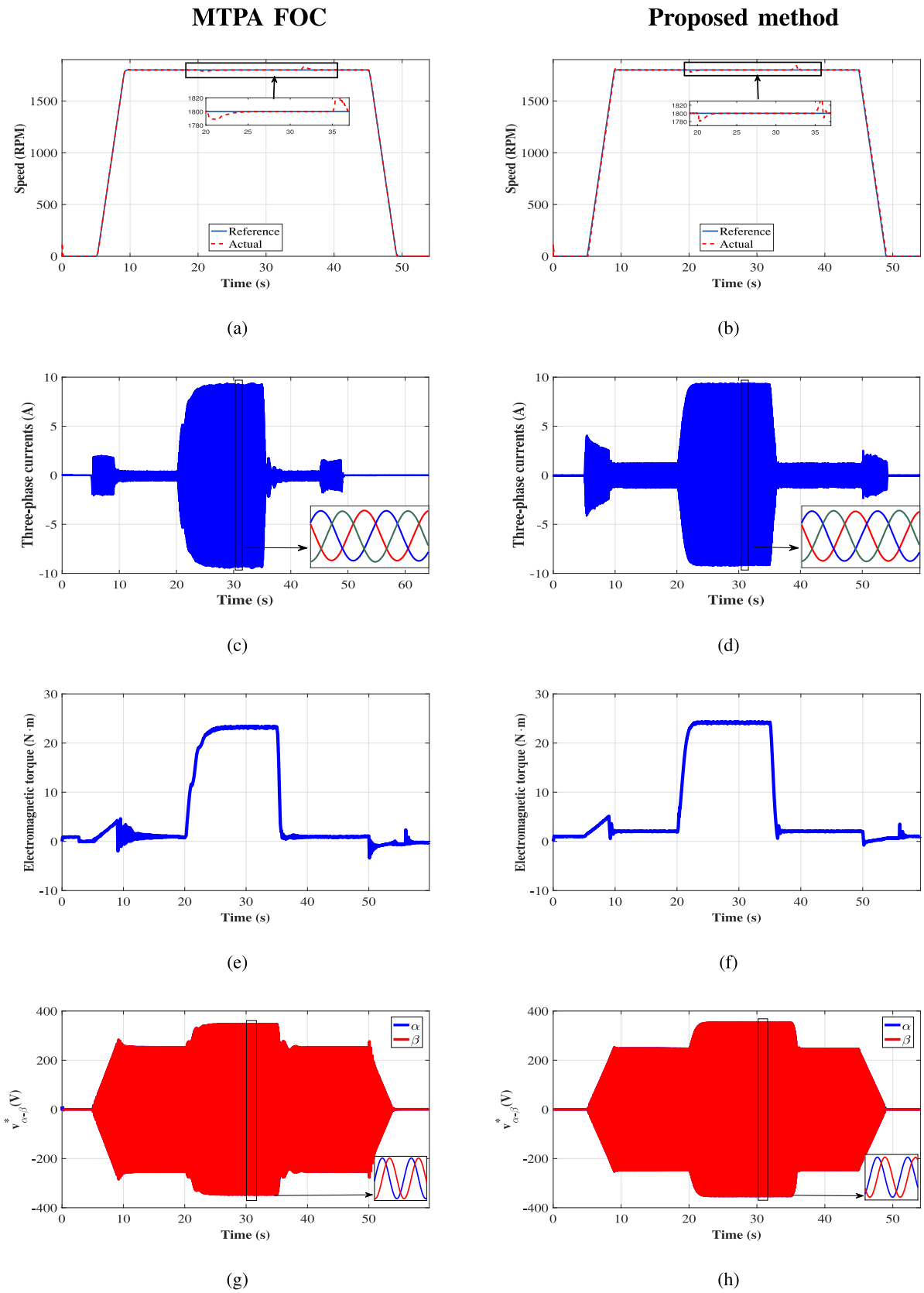

Fig. 6. Experimental results under 22 N·m at 1800 r/min. (a), (b) Reference and actual speed signals. (c), (d) Three-phase currents. (e), (f) Torque. (g), (h) Control voltages in the α–β reference frame.

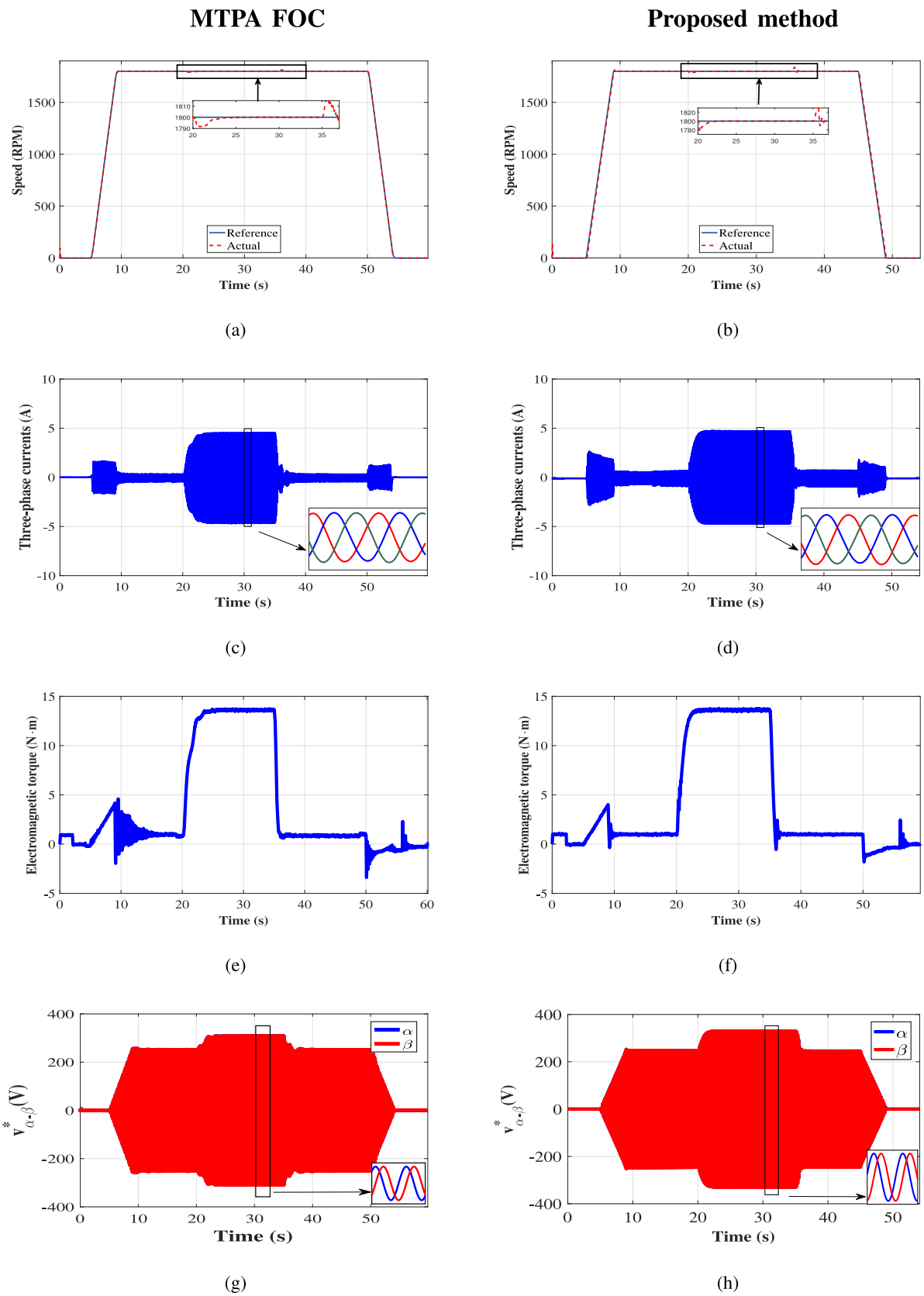

Fig. 7. Experimental results under 13 N·m at 1800 r/min. (a), (b) Reference and actual speed signals. (c), (d) Three-phase currents. (e), (f) Torque. (g), (h) Control voltages in the α–β reference frame.

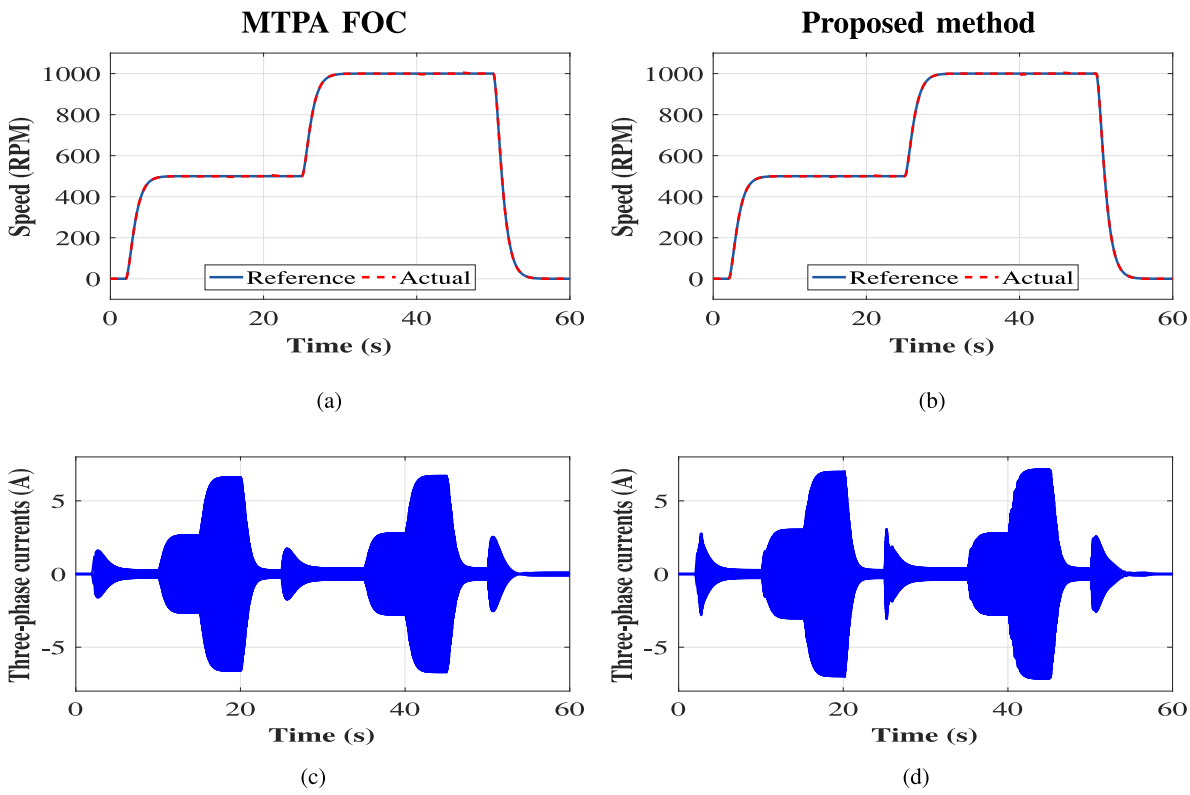

Fig. 8. Experimental results under various speed and load conditions. (a), (b) Reference and actual speed signals. (c), (d) Three-phase currents.

IV. Conclusion

In this paper, a simplified speed control scheme is developed for PMSMs without current sensing or motor's parameter knowledge. The proposed approach achieves speed tracking with direct voltage control avoiding the need of current sensing and control. As such, the control structure is simplified significantly compared to cascaded-based control techniques, such as vector control. To ensure optimal current consumption despite of the absence of current sensors, a GA-based optimization technique is presented to determine the set of control gains with a minimal current usage. Various simulations and experiments are carried out to validate its effectiveness at different operating conditions. Results show a good transient performance under load torque disturbance, using minimum current. This control scheme finds use in industrial motor drive applications with need of a robust controller to changing operating conditions and yet simple enough for practical low-cost implementation.

References

[1] M. Pinilla and S. Martinez, "Selection of main design variables for low-speed permanent magnet machines devoted to renewable energy conversion," *IEEE Trans. Energy Convers.*, vol. 26, no. 3, pp. 940–945, Sep. 2011.

[2] Y. Nyanteh, C. Edrington, S. Srivastava, and D. Cartes, "Application of artificial intelligence to real-time fault detection in permanent-magnet synchronous machines," *IEEE Trans. Ind. Appl.*, vol. 49, no. 3, pp. 1205–1214, May 2013.

[3] S. K. Kommuri, M. Defoort, H. R. Karimi, and K. C. Veluvolu, "A robust observer-based sensor fault-tolerant control for PMSM in electric vehicles," *IEEE Trans. Ind. Electron.*, vol. 63, no. 12, pp. 7671–7681, Dec. 2016.

[4] W. Kim, C. Yang, and C. C. Chung, "Design and implementation of simple field-oriented control for permanent magnet stepper motors without DQ transformation," *IEEE Trans. Magn.*, vol. 47, no. 10, pp. 4231–4234, Oct. 2011.

[5] Z. Wang, J. Chen, M. Cheng, and K. T. Chau, "Field-oriented control and direct torque control for paralleled VSIs fed PMSM drives with variable switching frequencies," *IEEE Trans. Power Electron.*, vol. 31, no. 3, pp. 2417–2428, Mar. 2016.

[6] Y. S. Choi, H. H. Choi, and J. W. Jung, "Feedback linearization direct torque control with reduced torque and flux ripples for IPMSM drives," *IEEE Trans. Power Electron.*, vol. 31, no. 5, pp. 3728–3737, May 2016.

[7] G. H. B. Foo and X. Zhang, "Constant switching frequency based direct torque control of interior permanent magnet synchronous motors with reduced ripples and fast torque dynamics," *IEEE Trans. Power Electron.*, vol. 31, no. 9, pp. 6485–6493, Sep. 2016.

[8] C. Xia, J. Zhao, Y. Yan, and T. Shi, "A novel direct torque control of matrix converter-fed PMSM drives using duty cycle control for torque ripple reduction," *IEEE Trans. Ind. Electron.*, vol. 61, no. 6, pp. 2700–2713, Jun. 2014.

[9] G. Prior and M. Krstic, "Quantized-input control Lyapunov approach for permanent magnet synchronous motor drives," *IEEE Trans. Control Syst. Technol.*, vol. 21, no. 5, pp. 1784–1794, Sep. 2013.

[10] Y.-C. Chang, C.-H. Chen, Z.-C. Zhu, and Y.-W. Huang, "Speed control of the surface-mounted permanent-magnet synchronous motor based on takagisugeno fuzzy models," *IEEE Trans. Power Electron.*, vol. 31, no. 9, pp. 6504–6510, Sep. 2016.

[11] S.-K. Kim, J.-S. Lee, and K.-B. Lee, "Self-tuning adaptive speed controller for permanent magnet synchronous motor," *IEEE Trans. Power Electron.*, vol. 32, no. 2, pp. 1493–1506, Feb. 2017.

[12] F. Niu, B. Wang, A. S. Babel, K. Li, and E. G. Strangas, "Comparative evaluation of direct torque control strategies for permanent magnet synchronous machines," *IEEE Trans. Power Electron.*, vol. 31, no. 2, pp. 1408–1424, Feb. 2016.

[13] M. Preindl and S. Bolognani, "Model predictive direct speed control with finite control set of PMSM drive systems," *IEEE Trans. Power Electron.*, vol. 28, no. 2, pp. 1007–1015, Feb. 2013.

[14] Z. Ma, S. Saeidi, and R. Kennel, "FPGA implementation of model predictive control with constant switching frequency for PMSM drives," *IEEE Trans. Ind. Informat.*, vol. 10, no. 4, pp. 2055–2063, Nov. 2014.
[15] A. Formentini, A. Trentin, M. Mar.esoni, P. Zanchetta, and P. Wheeler, "Speed finite control set model predictive control of a PMSM fed by matrix converter," *IEEE Trans. Ind. Electron.*, vol. 62, no. 11, pp. 6786–6796, Nov. 2015.
[16] S. Chai, L. Wang, and E. Rogers, "A cascade MPC control structure for a PMSM with speed ripple minimization," *IEEE Trans. Ind. Electron.*, vol. 60, no. 8, pp. 2978–2987, Aug. 2013.
[17] C. S. Lim, N. A. Rahim, W. P. Hew, and E. Levi, "Model predictive control of a two-motor drive with five-leg-inverter supply," *IEEE Trans. Ind. Electron.*, vol. 60, no. 1, pp. 54–65, Jan. 2013.
[18] H. Liu and S. Li, "Speed control for PMSM servo system using predictive functional control and extended state observer," *IEEE Trans. Ind. Electron.*, vol. 59, no. 2, pp. 1171–1183, Feb. 2012.
[19] J. R. Domnguez, A. Navarrete, M. A. Meza, A. G. Loukianov, and J. Caedo, "Digital sliding-mode sensorless control for surface-mounted PMSM," *IEEE Trans. Ind. Informat.*, vol. 10, no. 1, pp. 137–151, Feb. 2014.
[20] X. Zhang and Z. Li, "Sliding-mode observer-based mechanical parameter estimation for permanent magnet synchronous motor," *IEEE Trans. Power Electron.*, vol. 31, no. 8, pp. 5732–5745, Aug. 2016.
[21] T. Bernardes, V. F. Montagner, H. A. Grndling, and H. Pinheiro, "Discrete-time sliding mode observer for sensorless vector control of permanent magnet synchronous machine," *IEEE Trans. Ind. Electron.*, vol. 61, no. 4, pp. 1679–1691, Apr. 2014.
[22] X. Zhang, L. Sun, K. Zhao, and L. Sun, "Nonlinear speed control for PMSM system using sliding-mode control and disturbance compensation techniques," *IEEE Trans. Power Electron.*, vol. 28, no. 3, pp. 1358–1365, Mar. 2013.
[23] J. W. Jung, V. Q. Leu, T. D. Do, E. K. Kim, and H. H. Choi, "Adaptive PID speed control design for permanent magnet synchronous motor drives," *IEEE Trans. Power Electron.*, vol. 30, no. 2, pp. 900–908, Feb. 2015.
[24] H. H. Choi, N. T. T. Vu, and J. W. Jung, "Digital implementation of an adaptive speed regulator for a PMSM," *IEEE Trans. Power Electron.*, vol. 26, no. 1, pp. 3–8, Jan. 2011.
[25] S. K. Kim, K. G. Lee, and K. B. Lee, "Singularity-free adaptive speed tracking control for uncertain permanent magnet synchronous motor," *IEEE Trans. Power Electron.*, vol. 31, no. 2, pp. 1692–1701, Feb. 2016.
[26] X. Song, J. Fang, B. Han, and S. Zheng, "Adaptive compensation method for high-speed surface PMSM sensorless drives of EMF-based position estimation error," *IEEE Trans. Power Electron.*, vol. 31, no. 2, pp. 1438–1449, Feb. 2016.
[27] J. Yu, P. Shi, W. Dong, B. Chen, and C. Lin, "Neural network-based adaptive dynamic surface control for permanent magnet synchronous motors," *IEEE Trans. Neural Netw. Learn. Syst.*, vol. 26, no. 3, pp. 640–645, Mar. 2015.
[28] F. J. Lin, I. F. Sun, K. J. Yang, and J. K. Chang, "Recurrent fuzzy neural cerebellar model articulation network fault-tolerant control of six-phase permanent magnet synchronous motor position servo drive," *IEEE Trans. Fuzzy Syst.*, vol. 24, no. 1, pp. 153–167, Feb. 2016.
[29] H. H. Choi, H. M. Yun, and Y. Kim, "Implementation of evolutionary fuzzy PID speed controller for PM synchronous motor," *IEEE Trans. Ind. Informat.*, vol. 11, no. 2, pp. 540–547, Apr. 2015.
[30] F. J. Lin, Y. C. Hung, and K. C. Ruan, "An intelligent second-order sliding-mode control for an electric power steering system using a wavelet fuzzy neural network," *IEEE Trans. Fuzzy Syst.*, vol. 22, no. 6, pp. 1598–1611, Dec. 2014.
[31] J. Yu, P. Shi, W. Dong, B. Chen, and C. Lin, "Neural network-based adaptive dynamic surface control for permanent magnet synchronous motors," *IEEE Trans. Neural Netw. Learn. Syst.*, vol. 26, no. 3, pp. 640–645, Mar. 2015.
[32] T. Pajchrowski, K. Zawirski, and K. Nowopolski, "Neural speed controller trained online by means of modified RPROP algorithm," *IEEE Trans. Ind. Informat.*, vol. 11, no. 2, pp. 560–568, Apr. 2015.
[33] H. Chaoui, M. Khayamy, and O. Okoye, "Adaptive RBF network based speed control for interior PMSM drives without current sensing," *IEEE Trans. Veh. Technol.*, to be published.
[34] P. D. C. Perera, F. Blaabjerg, J. K. Pedersen, and P. Thogersen, "A sensorless, stable V/f control method for permanent-magnet synchronous motor drives," *IEEE Trans. Ind. Appl.*, vol. 39, no. 3, pp. 783–791, May 2003.
[35] Z. Tang, X. Li, S. Dusmez, and B. Akin, "A New V/f-based sensorless MTPA control for IPMSM drives," *IEEE Trans. Power Electron.*, vol. 31, no. 6, pp. 4400–4415, Jun. 2016.
[36] A. Ahmed, Y. Sozer, and M. Hamdan, "Maximum torque per ampere control for buried magnet PMSM based on DC-link power measurement," *IEEE Trans. Power Electron.*, vol. 32, no. 2, pp. 1299–1311, Feb. 2017.
[37] H. Chaoui and P. Sicard, "Adaptive fuzzy logic control of permanent magnet synchronous machines with nonlinear friction," *IEEE Trans. Ind. Electron.*, vol. 59, no. 2, pp. 1123–1133, Feb. 2012.
[38] H. Chaoui, M. Khayamy, and A. Aljarboua, "Adaptive interval type-2 fuzzy logic control for PMSM drives with a modified reference frame," *IEEE Trans. Ind. Electron.*, vol. 64, no. 5, pp. 3786–3797, May 2017.
[39] J.-J. Chen and K.-P. Chin, "Automatic flux-weakening control of permanent magnet synchronous motors using a reduced-order controller," *IEEE Trans. Power Electron.*, vol. 15, no. 5, pp. 881–890, Sep. 2000.
[40] H. Chaoui, O. Okoye, and M. Khayamy, "Current sensorless MTPA for IPMSM drives," *IEEE/ASME Trans. Mechatronics*, vol. 22, no. 4, pp. 585–1593, Aug. 2017.
[41] A. D. Alexandrou, N. K. Adamopoulos, and A. G. Kladas, "Development of a constant switching frequency deadbeat predictive control technique for field-oriented synchronous permanent-magnet motor drive," *IEEE Trans. Ind. Electron.*, vol. 63, no. 8, pp. 5167–5175, Aug. 2016.
[42] K. C. Kim, "A novel magnetic flux weakening method of permanent magnet synchronous motor for electric vehicles," *IEEE Trans. Magn.*, vol. 48, no. 11, pp. 4042–4045, Nov. 2012.
[43] C. Zhou *et al.*, "An improved direct adaptive fuzzy controller of an uncertain PMSM for web-based e-service systems," *IEEE Trans. Fuzzy Syst.*, vol. 23, no. 1, pp. 58–71, Feb. 2015.
[44] S. Bozhko, S. Dymko, S. Kovbasa, and S. M. Peresada, "Maximum torque-per-amp control for traction IM drives: Theory and experimental results," *IEEE Trans. Ind. Appl.*, vol. 53, no. 1, pp. 181–193, Jan. 2017.
[45] F. Xu, L. Shi, and Y. Li, "The weighted vector control of speed-irrelevant dual induction motors fed by the single inverter," *IEEE Trans. Power Electron.*, vol. 28, no. 12, pp. 5665–5672, Dec. 2013.
[46] M. Preindl and S. Bolognani, "Optimal state reference computation with constrained MTPA criterion for PM motor drives," *IEEE Trans. Power Electron.*, vol. 30, no. 8, pp. 4524–4535, Aug. 2015.
[47] H. Chaoui and P. Sicard, "Adaptive fuzzy logic control of permanent magnet synchronous machines with nonlinear friction," *IEEE Trans. Ind. Electron.*, vol. 59, no. 2, pp. 1123–1133, Feb. 2012.
[48] K. Liu and Z. Q. Zhu, "Quantum genetic algorithm-based parameter estimation of PMSM under variable speed control accounting for system identifiability and vsi nonlinearity," *IEEE Trans. Ind. Electron.*, vol. 62, no. 4, pp. 2363–2371, Apr. 2015.

Hicham Chaoui (S'01–M'12–SM'13) received the Ph.D. degree (Hons.) in electrical engineering from the University of Quebec, Trois-Rivières, QC, Canada, in 2012.

His career has spanned both academia and industry in the field of control and energy systems. From 2007 to 2014, he held various engineering and management positions in the Canadian industry. From 2014 to 2016, he was an Assistant Professor at Tennessee Technological University, Cookeville, TN, USA. Since then, he has been a Faculty Member at Carleton University, Ottawa, ON, Canada. His research interests include adaptive and nonlinear control theory, intelligent control, robotics, electric motor drives, and energy conversion and storage systems. He has authored or coauthored more than 100 journal and conference publications.

Dr. Chaoui was a recipient of the Best Thesis Award and the Governor General of Canada Gold Medal Award. He is a Registered Professional Engineer in the Province of Ontario. He is also an Associate Editor for IEEE TRANSACTIONS ON VEHICULAR TECHNOLOGY.

Mehdy Khayamy was born in Ahvaz, Iran. He received the B.Sc. degree in electrical engineering from Chamran University of Ahvaz, Iran, in 2004, the M.Sc. degree in electrical engineering from University of Tehran, Tehran, Iran, in 2008, and the Ph.D. degree in electrical engineering from Tennessee Technological University, Cookeville, TN, USA, in 2017.

His masters and doctoral research are focused on power electronics and the development of control algorithms for control of electric machines and control of control power electronic converters for solar and wind renewable energy systems and battery application. He was a Senior Test Engineer of high power converters and a Planner Engineer in an oil refinery industry. He authored or coauthored a book on the application of MATLAB in mathematics.

Okezie Okoye was born in Lagos, Nigeria. He received the bachelor's degree in electronic and electrical engineering from Obafemi Awolowo University, Ife, Nigeria, in 2013, and the master's degree in electrical engineering from Tennessee Technological University, Cookeville, TN, USA, in May 2017.

His master's research work has produced more than five journal and conference publications. Mr. Okoye is currently with Cummins Inc., Columbus, IN, USA. His research interests include renewable energy systems, power electronics, and electric machine drives.

Hamid Gualous (M'14) received the Ph.D. degree in electronics from the University of Paris XI, Orsay, France, in 1994.

From 1996 to 2009, he was an Associate Professor with the University of Franche-Comte, FEMTO-ST Laboratory, France. He is currently a Full Professor with the University of Caen-Normandie, Cherbourg-Octeville, France and the Director of LUSAC Laboratory, Cherbourg-Octeville, France. His main research activities include energy storage device, marine renewable energies, and energy management systems for smart grids.